Two-phase flow patterns investigation in large aspect ratio microchannel with T-mixer

Yuriy Dementyev[1], Evgeniy Chinnov[1], Fedor Ronshin[1], Anatoliy Evstrapov[2] and Victor Gusev[2]*
[1]*Kutateladze Institute of Thermophysics, 630090 Novosibirsk, Russia*
[2]*Institute for Analytical Instrumentation RAS, 190103, St.Petersburg, Russia*

Abstract. Two-phase flows in microchannels have a wide range of applications in various fields of science and technology (cooling of electronic equipment, microfluidics, micromixers, etc.). Two-phase flows in microchannels with characteristic sizes on the order of 10 μm and below becomes an important object of study due to new effects that are realized on this scale. In this work, we study a two-phase flow in a slit microchannel 10 μm height and 10 mm wide, where the liquid was injected coaxially to the two-phase flow and the gas was injected perpendicular to the two-phase flow. The realized flow patterns (Jets and Jet-Droplet, Churn and Droplet-Annular) and their boundaries are determined and described. The mechanisms of liquid jets amount evolution are shown and described. The flow pattern maps have been compared with ones for phase input inversion. The influence of the mixer on the boundaries of flow patterns is described.

1 Introduction

In the last two decades, in fact, there has been a revolutionary development of heat exchange systems with mini-, micro- and nano-sizes, and these systems turn out to be much more energy efficient than macro-systems with channel sizes of 3–100 mm. The value of the removed heat fluxes in the created mini- and micro-heat exchangers can reach 1000 W/cm^2 and more. Also in the last few years there has been an intensive development of 3D chips, where it is necessary to remove heat directly from the chip. The most promising cooling solution seems to be the use of microchannels that are brought inside the chip, directly to the heat generating element. A significant enhancement of heat transfer occurs in processes with a phase transition (boiling, evaporation). For understanding the processes with phase transitions in microchannels, it is also necessary to study flows under adiabatic conditions, since these studies provide information on flow characteristics, such as pressure drop, void fraction, flow patterns, film thickness etc. Also, enhancement of heat transfer in microchannel gas-liquid heat exchange systems can be achieved by reducing the thickness of the liquid film in contact with a solid heat-generating surface. In this case, a decrease in the typical channel size also leads to a decrease in the film thickness, which leads to an intensification of heat transfer during evaporation [1]. In this regard, microchannels with a height of about 10 μm are the most promising, since the characteristic thicknesses of liquid films are less than 1 μm.

Also, over the past two decades, methods for creating microstructures up to sizes of the order of tens of nanometers have been actively developed. The papers [2-4] present technologies for creating microstructures for microfluidic chips, such as sintering, bonding, UV glue, solvent chemical bonding, laser ablation and thermal sintering methods.

Adiabatic two-phase flows in mini- and microchannels have been actively studied in the last two decades. Researchers mainly focus on the study of flow patterns and their boundaries, two-phase pressure drop and the influence of channel geometry. In the work [5] presented the review of instabilities affecting two-phase flow in microsystems. In the work [6] the effects of surface wettability in rectangular microchannels on two-phase flow characteristics have been studied. It was shown that the two-phase flow patterns were highly affected by surface wettability. In the hydrophilic microchannel, the major flow patterns were bubbly, elongated bubble and liquid ring flow. In the hydrophobic microchannel, the major flow pattern was stratified flow, which was governed by capillary force and hydrophobicity. Sur and Liu [7] investigated round channels with diameters of 100, 180 and 324 μm. It has been established that the boundaries of the flow patterns shift with decreasing channel diameter mainly as a result of competition between inertial forces and surface tension. A new flow pattern map using modified Weber numbers as coordinates has been developed in order to unify transition lines between flow patterns in microchannels of different sizes. The authors also studied pressure drop and showed that two-phase frictional pressure drop can be predicted more accurately with models based on flow structure than with homogeneous and separate flow models. Bartkus et al. [8] studied gas–liquid flow of an ethanol–nitrogen mixture in a 390x150 μm² microchannel with variations in the frequency and amplitude of the external pulsations of the liquid flow rate. The experiments were carried out with external pulsations of a sinusoidal waveform at

liquid flow rates f = 1 and 2 Hz and different amplitude values. The imposition of external pulsations of the liquid flow rate in the slug flow regime with narrow distributions of the bubble size and velocity led to significant broadening of the bubbles.

The review of two-phase flow studies in channels of different geometries and sizes is presented in the works of [9,10]. In the work [11], rectangular channels 50-200 µm high with a large aspect ratio (channel widths 10-20 mm) were studied. Flow patterns were found that do not occur in square and round channels, namely, Stratified Wave and Jet.

2 Experimental Setup

The working section consists of a flow cell and an injection frame. The injection frame was manufactured of stainless steel and it was a metal component with threaded holes for fittings and pressure sensors. The flow cell consisted of two glass plates (lower and upper) made of Borofloat®33 optical borosilicate glass with dimensions of 75x20x3.8 mm^3 and a monocrystalline silicon wafer with dimensions of 75x20x0.48 mm^3, in which a microchannel structure was etched. Before the photolithography process, holes with a diameter of 10 mm were manufactured in the lower glass plate for phases injection and for removal of a two-phase mixture. A protective mask of silicon nitride (Si_3N_4) was formed on a silicon wafer by photolithography to form a v-groove. Then, using deep anisotropic etching, a v-shaped groove was etched to a depth of 440-470 µm, which became a gap for gas injection to the channel. For anisotropic etching, the orientation of the initial silicon wafer is significantly important. We chose (100) because when such silicon is etched, the walls of the etching region are formed at an angle of 54.7°. For etching, an aqueous solution of 45% potassium hydroxide (KOH) was used, its temperature was maintained stable (85°C) throughout the entire process using a water bath. Thereby, it was possible to achieve a stable etching rate of 1.8–1.9 µm/min. The wafer was immersed in the solution for a period of 4.5 to 5 hours, until the walls closed and a v-shaped groove formed. The transverse size of the gap was chosen to provide enough etching depth for closing the v-groove to for further etching of the 0.01x10 mm^2 microchannel on the reverse side of the silicon wafer to immediately open a through gap about 5-7 µm size. The microchannel 0.01x10 mm^2 on the reverse side of the silicon wafer is also formed using photolithography. Then the wafer with the Si_3N_4 protective mask and a small layer (0,3 µm) of SiO_2 was immersed in the Plasmalab100 plasma-chemical etching setup, and the etching was carried out in a fluorine plasma (SF_6). This method was chosen because it allows to obtain reproducible dimensions of the pattern without damaging the reverse side of the wafer. During the etching process, the silicon wafer was periodically removed to control the width of the gap and the depth of microchannel etching. The etching time was 12-15 minutes.

Further, holes were cut in the silicon wafer with a help laser to form the liquid inlet and the two-phase mixture outlet. After the fabrication of all microstructures, the lower glass plate was sealed with a silicon wafer by thermal anode bonding. Next, the upper glass plate with silicon was sealed in a similar way. The physical principle of thermal anode bonding is as follows. For definite modification of the glass properties, certain oxides impurities are introduced into the quartz mixture. In our case (for Borofloat33) these are B_2O_3, Al_2O_3, K_2O, Na_2O. Under the action of temperature, partial dissociation of oxides occurs. The K_2O and Na_2O oxides have the lowest activation energy of this process:

$$K_2O \rightarrow 2K^+ + O^- + 288\ кJ$$
$$Na_2O \rightarrow 2Na^+ + O^- + 299кJ$$

Further, under the action of an electric field, the ions are redistributed in the volume. Oxygen moves to the interface with silicon, where it is oxidized, forming an inseparable bond with glass.

Bonding modes can be very different and depend on the equipment used. In our case, bonding was carried out at 430-450 °C at a speed of approximately 10 deg/min at a voltage of 800-1000 V and a holding time of 50 minutes when the upper plate with a silicon substrate bonded. Before bonding the lower plate, the already bonded module of silicon wafer and the upper glass plate was chemically treated. Further, the two-layer module was bonded with the lower glass plate at higher voltages of 1000-1200 V. Bonding was carried out in clean industrial premises (cleanliness class not less than 7 14644 ISO). The sealing area was more than 95% percent of the total contact area.

The injection frame was connected to the flow cell using Loctite® 460 cyanoacrylate adhesive (without bloom effect) and kept for a day before the experiment. A photograph of the test section is shown in Fig.1. The final dimensions of the microchannel: height - 10 µm, width - 10 mm, distance from the center of the liquid inlet hole to the gas injection gap - 35 mm (gas zone), from the gas injection gap from the center of the outlet hole (two-phase zone) - 25 mm, holes diameter -10 mm, gas injection gap ~5-7 µm x 8 mm.

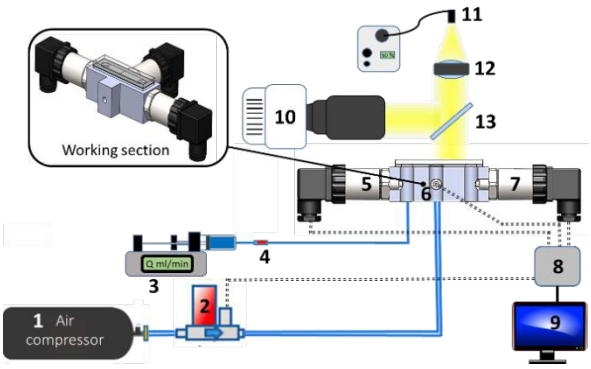

Fig 1. Experimental setup. 1-air compressor, 2 – gas flow controller, 3 – syringe pump, 4- 202 nm membrane filter, 5,6,7 – pressure sensors, 8 – controller, 9 – computer, 10 – camera, 11 – light source, 12 –lens, 13-50/50 beam splitter.

The scheme of the experimental setup is shown in Fig.3. Gas was injected to the test section from an air compressor (1) through a Bronkhorst® EL-FLOW F211CV gas flow controller (2) (measured flow rates from 2 to 100 ml/min), controlled using National

Instruments® LABVIEW software in a computer (9). Liquid was injected using a Cole-Parmer® EW-74905-54 digital syringe pump (3) through a 202 nm membrane syringe filter (4). Pressure sensors DMP 331 of BD sensors® company (5,6,7) were screwed into the injection frame to measure the differential pressure. The signals from the pressure sensors and the gas flow regulator were sent to the National Instruments® DAQ-mx USB-6001 controller (8) and then to the computer (9). The signals of the pressure sensors and the gas flow regulator were monitored using the National Instruments® LABVIEW software. The flow was visualized using a schlieren system consisting of a powerful light source Olympus® KL 2500 LED (11), focusing lens (12), 50/50 beam splitter (13) and a Nikon® D500 camera (shooting frequency 60 frames per second) with Nikon® AF-S VR Micro-Nikkor 105mm f/2.8G IF-ED lens (10). Details of visualization of two-phase flows with the schlieren system are described in [12].

Before the experiment, the roughness of channel surfaces was measured. The average roughness for silicon with 0,3 µm SiO_2 layer sample was 4 nm and for Borofloat® 33 glass sample was 7.8 nm. The fluid properties presented in table 1.

Table 1. Working fluid properties

	Density, [kg/m³]	Dynamic viscosity [Pa·s]	Wettability contact angle θ, °	Surface tension [N/m]
HFE-7100	1520	$5.7\cdot10^{-4}$	<5°	$13.6\cdot10^{-3}$
Air	1.2	$1.83\cdot10^{-5}$		

3 Results and discussion

3.1 Flow patterns

Jets and Jet-Droplet flow patterns

At low and middle liquid and gas superficial velocities U_{sl} and U_{sg} determined as the ratio of volumetric flow rate of the phase Q_{ph} to cross sectional area S of the channel, alternating Jet and Jet-Droplet flow patterns were observed. This patterns are characterized by alternating liquid and gas jets along the channel width. The amount and size of the jets depend on the superficial liquid and gas velocities. Simultaneously, situations where there is a stable liquid jet and jet nuclei from which droplets detach can exist. Fig. 2 shows the evolution of liquid jets amount at gas superficial velocity increasing. It is seen that with increasing of superficial gas velocity the amount of liquid jets decreases at U_{sl} = 0.083 m/s and 0.02 m/s, however increase at U_{sl} = 0.05 m/s. Thus, there are two mechanisms of liquid jets amount evolution.

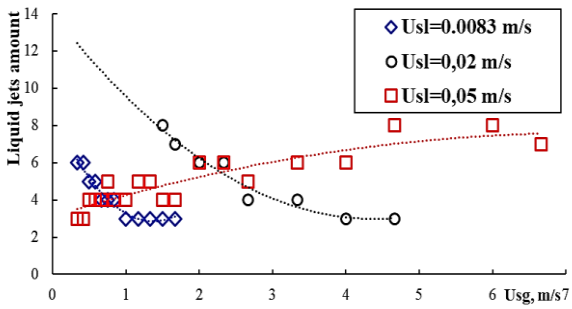

Fig.2. Liquid jets amount versus gas superficial velocity U_{sg}.

In the first case (Fig.3), the liquid volume fraction in the channel is small, i.e. the liquid acts as the dispersed phase, and the gas as the carrier. With an increase of gas superficial velocity U_{sg}, the amount of liquid jets that were initially formed in the mixing zone decreases due to an increase in the gas volume fraction. At the first stage, drops break off along the single liquid jet, forming jet-droplet flow pattern (Fig. 3b). Then the liquid jet completely disappears due to gas displacement (Fig. 3c). Fig.3 shows jets and jet-droplet flow patterns at U_{sl} = 0.02 m/s and U_{sg} = 1.5 m/s (a) at U_{sl} = 2.3 m/s (b) and U_{sl} = 4 m/s (c). In the second case at high superficial velocities of liquid (U_{sl} = 0.05 m/s), liquid volume fraction in the channel is large, especially in the center of channel. With further increasing of gas superficial velocity new gas jets are formed (Fig. 4b, 4c). At the same time, the amount of liquid jets grows due to the breaking of one large liquid jet into smaller ones (Fig. 4b, 4c).

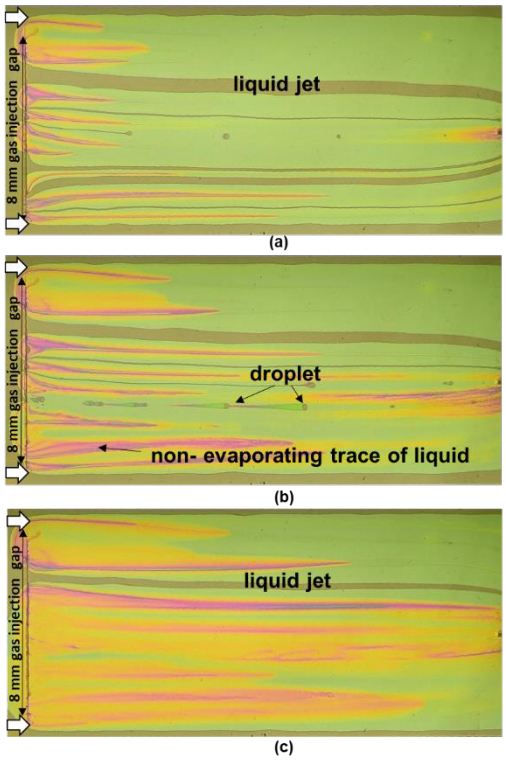

Fig 3. Jets and jet-droplet flow patterns at U_{sl} = 0.02 m/s (a) U_{sg} = 1.5 m/s (b) U_{sg} = 2.3 m/s (c) U_{sg} = 4 m/s.

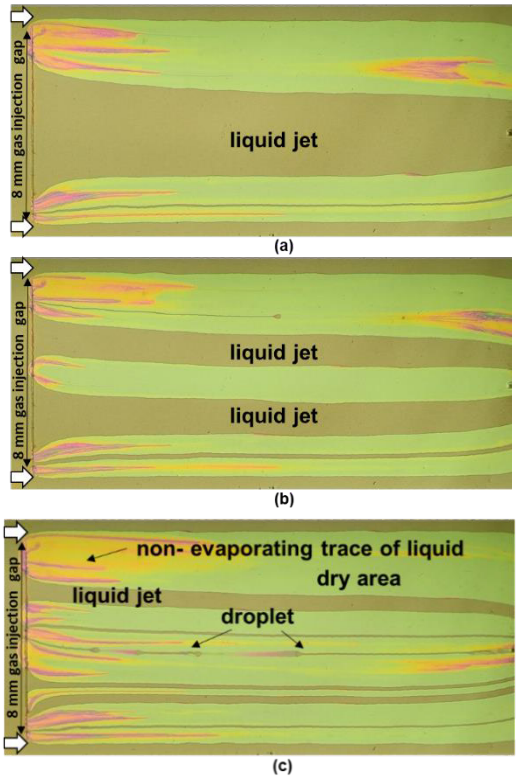

Fig 4. Jets and jet-droplet flow patterns at U_{sl} = 0.05 m/s, (a) U_{sg} =1.5 m/s (b) U_{sg} = 2 m/s (c) U_{sg} = 4.66 m/s.

Churn flow pattern

At high superficial liquid velocities U_{sl} and at low and middle superficial velocities of gas U_{sg} Churn flow pattern was observed. At this flow several types of instabilities develop along gas jets forming gas conglomerates of complex shape. Developed instabilities are instability caused by transverse pressure gradient, which force conglomerates forming along side jets and Saffman-Taylor instability, which is formed complex shape conglomerates due to viscous fingers. Viscous fingers penetrate gas bubble, forming gas-liquid structures of complex shape. Conglomerates formed along different jets merge due to the transverse pressure gradient. At this pattern, an interference film not closed along channel width is visualized on the upper wall of the channel. Moreover, the dispersed and carrier phases are difficult to distinguish. Fig.5 shows Churn flow pattern at U_{sl} =0.25 m/s and U_{sg} = 0.75 m/s.

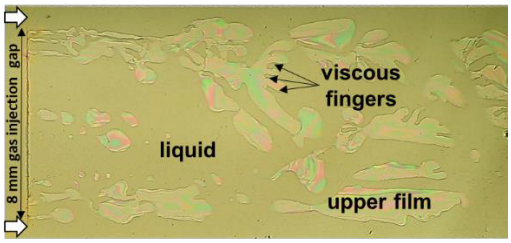

Fig 5. Churn flow pattern at U_{sl} = 0.25 m/s and U_{sg} = 0.75 m/s

Droplet-Annular flow pattern

At high lquid U_{sl} and gas U_{sg} superficial velocities Droplet-Annular flow pattern was observed. At this pattern liquid droplets move in the gas core when gas is carrier phase and liquid is dispersed phase. Wherein, liquid droplets do not break the liquid film along or across the direction of flow. At the center of channel pieces of liquid and droplets larger than along the side.

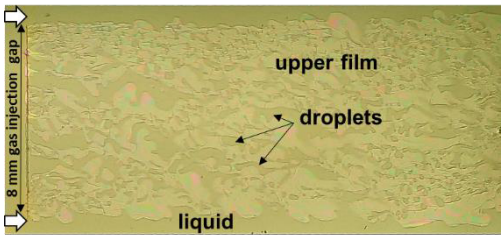

Fig 6. Droplet-Annular flow pattern at U_{sl} = 0.216 m/s and U_{sg} = 5 m/s.

3.2 Flow pattern maps

Fig.7 shows flow pattern map and flow pattern borders for channel 0.01x10 mm^2 where gas and liquid superficial velocities were used as coordinates. Fig. 8 shows the comparison of 0.01x10 mm^2 channel for investigated flow configuration with flow pattern map of the same channel but with inverse phase inlets, i.e. the gas was injected coaxially to the two-phase flow, and the liquid was injected at an angle of 90°.

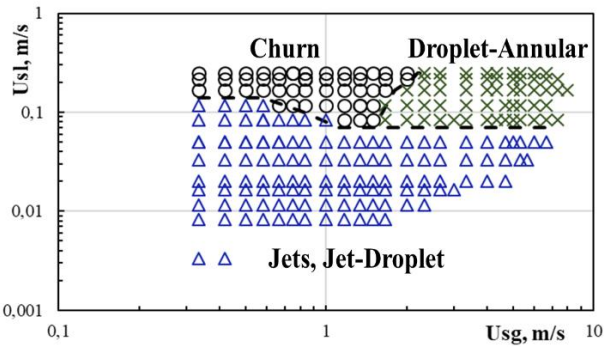

Fig .7 Flow pattern map of HFE-7100-air of 0.01x10 mm².

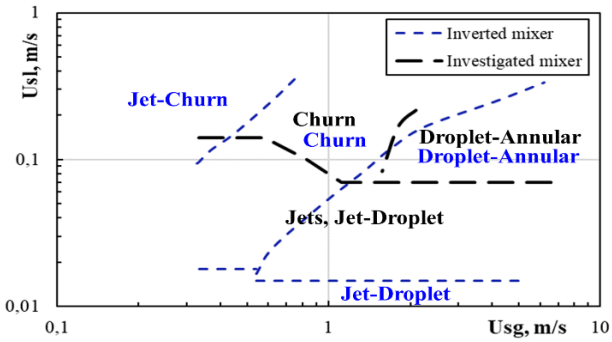

Fig. 8 Comparison of flow pattern maps for 0.01x10 mm², Black lines –borders of investigated mixer (liquid injection coaxially to the two-phase flow, gas – perpendicular to the two-phase flow). Blue lines – borders of inverted mixer (gas injection coaxially to the two-phase flow, liquid-parpendicular to the two-phase flow)

Fig. 8 shows that the flow patterns are almost identical when the mixer is inverted. The investigated mixer increases the region of Jets and Jet-Droplet flow patterns towards higher superficial liquid velocities. Moreover, in the investigated flow configuration, there is no Jet-Churn flow pattern. The Jet-Churn flow pattern was formed in the case of the inverse mixer when two

gas jets flow past a liquid meniscus in the mixing zone along the side walls of the channel. In this case, a pulsating transverse instability was formed at the interfaces, directed towards the center of the channel. This instability formed gas conglomerates that did not merge with each other. With a further increase of gas superficial velocity, the conglomerates merged, forming Churn flow pattern. In the investigated mixer configuration, three or more gas flow centers are immediately appeared, forming Churn flow pattern directly.

Conclusions

In this work, we studied the two-phase flow in a short slit microchannel 10 μm height and 10 mm wide, where the liquid was injected coaxially to the two-phase flow and the gas was injected perpendicular to the two-phase flow. HFE-7100 was used as a working fluid, and air was used as a working gas. With help of schlieren optical system tree flow patterns have been visualized and described: Jets and Jet-Droplet, Churn and Droplet-Annular. In the Jets and Jet-Droplet flow mechanisms of liquid jets amount evolution are shown and described. In the first case, the liquid volume fraction in the channel is small, i.e. the liquid acts as the dispersed phase, and the gas as the carrier. With an increase of superficial gas velocity, the amount of liquid jets that were initially formed in the mixing zone decreases due to an increase in the gas volume fraction. At the first stage, drops break off along the single liquid jet, forming Jet-Droplet flow pattern. Then the liquid jet completely disappears due to gas. In the second case at high superficial velocities of liquid, liquid volume fraction in the channel is large, especially in the center of channel. With further increasing of gas superficial velocity new gas jets are formed. At the same time, the amount of liquid jets grows due to the breaking of one large liquid jet into smaller ones. The comparison of the flow patterns boundaries with the boundaries of flow pattern map realized with phase input inversion has been made. The influence of the mixer on the boundaries of flow patterns has been investigated. The investigated mixer increases the region of Jets and Jet-Droplet flow patterns towards higher superficial liquid velocities. Moreover, it was shown that in the investigated flow configuration, there is no Jet-Churn flow pattern due to three or more gas flow centers are immediately appear, forming Churn flow pattern directly in contrast to the configuration with an inverse mixer.

The study was carried out within the framework of the state task No.121031800213-0

References

1. O.A. Kabov, Y.V. Lyulin, I.V. Marchuk, D.V. Zaitsev. Int. J. Heat Fluid Flow, **28** (1), 103 (2007).
2. T.A. Lukashenko, A.N. Tupik, G.E. Rudnitskaya, A.L. Bulyanitsa, A.I. Tsymbalov, A.A. Evstrapov. Naychnoe priborostroenye [Scientific Instrumentation], **26** (2), 64 (2016) (in Russian)
3. A.A. Evstrapov, T.A. Lukashenko, C.G. Gornuy, K.V. Yudin, Naychnoe priborostroenye [Scientific Instrumentation], **15** (2), 72 (2005) (in Russian)
4. A.A. Evstrapov, T.A. Lukashenko, A.N. Tupik. [Scientific Instrumentation], **20** (1), 29 (2010) (in Russian)
5. L.E. O'Neill, I. Mudawar. Int. J. Heat Mass Transf. **157**, 119738 (2020)
6. C. Choi, D.I. Yu, M. Kim. Exp. Therm. and Fluid Sci. **35** (6), 1086 (2011)
7. A. Sur, D. Liu, Int. J. Thermal Sciences **53**, 18 (2012)
8. G.V. Bartkus, A.V. Kovalev, A.A. Yagodnitsyna. Interfacial Phenomena and Heat Transfer **11**, 1 (2023)
9. E.A. Chinnov, O.A. Kabov, High Temp. **44** (5), 773 (2006)
10. E.A. Chinnov, F.V. Ronshin, O.A. Kabov, Thermophysics and Aeromechanics, **22** (3), 265 (2015)
11. E.A. Chinnov, F.V. Ron'shin, O.A. Kabov, Interfacial Phenomena and Heat Transfer **3** (3), 243 (2015)
12. F.V. Ron'shin, V. Cheverda, E. Chinnov, O.A. Kabov. Interfacial Phenomena and Heat Transfer **4** (2-3), 191 (2016)